Organic Complex Structures: Contemporary Designs and Future Potential

Zhenxiang Xu[1]

Yingli Shi[1, 2, *]

[1] School of Advanced Technology, Xi'an Jiaotong-Liverpool University, Suzhou 215123, China

[2] Department of Electrical Engineering and Electronics, University of Liverpool, Liverpool L69 3GJ, UK.

[*] Yingli.Shi@xjtlu.edu.cn

Abstract

With the development of electronic devices, the organic complex structure serves a crucial function in the photonic device area due to its tunable optoelectronic properties as well as mechanical flexibility, while the performance of simple structure materials is limited due to their overly simplistic architecture. In recent years, researchers have dedicated significant efforts to the fabrication of organic micro/nano-crystal fabrication, specially improving design and construction methods to prompt to get well-behaved organic complex structure which could be used in optoelectronic applications. In this review, the recent development of organic micro/nanocrystals with complex structures along with representative works s are discussed with a specific focus on molecular design, synthesis, and advanced applications. Additionally, we also provide a concise summary and perspective on the potential future research directions regarding organic crystals with complex structures, highlighting their promising role in photonic integrated circuits.

1. Introduction

Since the invention of the first polythiophene field-effect transistor in 1986[1], organic field-effect transistors have undergone rapid development. The research in organic semiconductor materials, devices, and fabrication processes has also achieved remarkable progress. Specifically, organic micro/nanocrystals have gained increasing attention in recent years due to their outstanding performance in electronic devices and their wide range of applications including organic field-effect transistors (OFETs),[2, 3] organic solid-state lasers (OSSLs),[4-7] organic light-emitting diodes (OLEDs),[8-10] organic photonic integrated circuits (OPICs)[11] and so on. Organic complex micro/nanostructures with tunable functionality and enhanced electrical and optical properties are considered to have significant potential. Furthermore, in comparison to more simplistic structures, complex structures are notably advantageous due to their unique architecture. These advantages include 1) enhanced suitability for achieving interconnectivity between units 2) increased flexibility in modifying molecular structures and 3) improved capacity for hosting a variety of functional groups. This makes them the ideal components for constructing multifunctional integrated circuits and processing signals for applications such as optical communication, photonic integrated circuits, and so on.

In the past few years, complex semiconductors based on inorganic materials such as ZnO[12], PbS[13],TiO2[14], have been extensively applied in sensors, optoelectronics and microelectronic devices. This extensive application has led to significant advancements, achieving great progress in these fields.[1214] For instance, Ramgir et al. demonstrated a TiO_2/ZnO heterostructure nanowire-based sensor for NO_2 detection, leveraging the unique properties of these materials for enhanced sensitivity and selectivity.[15] Xu et al. reported on the fabrication of high-performance carbon-based all-inorganic solar cells using a PbS/CdS heterojunction thin layer which could significantly enhance solar cell's efficiency[16] and Pei and Zhai reported using MoS_2 and graphene with organic molecules to create heterojunctions which enhanced electronic functions[17]. However, mere physical juxtaposition at the heterojunction interface results in significant lattice dissonance and subsequent optical inefficiencies. Compared to inorganic complex structures, organic complex structures, due to their unique customizability at the molecular level and designability at the structural level, they possess the following advantage:1) Precise customization at the molecular level. 2) Adaptability to diverse conditions. 3) Low-cost processing. 4) Eco-friendly sourcing and production. 5) Simple preparation method.
Recently, organic semiconductor micro/nanostructures have become a hot research topic due to their diversity and flexibility in molecular design and synthesis, excellent physical/chemical properties, and low-cost large-area preparation. In contrast, the fine synthesis of complex micro/nanostructures with different components/substructures faces greater challenges that must be overcome to meet the requirements of practical nanotechnology. In this review, we primarily focus on giving a new perspective for categorizing these complex structures based on different dimensional combinations as well as introducing the growth mechanism of these complex structures. Subsequently, we classify and compare recent fabrication methods for functional optical microdevices based on these structures. Then we offer a perspective on the further development and application of organic complex structures, particularly in the future of optical logic, anti-counterfeiting, and organic photonic integrated circuits (OPICs). Finally, we will summarize the challenges in organic complex structure and give a future development outlook for these challenges.

2. Categories

Classification

In this essay, we categorize organic complex structures mainly into flexible complex structures and non-flexible complex structures with different dimensions. In detail, non-flexible crystals can be further devided into complex structures with dimensions less than or equal to one dimension and two-dimensional complex structures. With respect to their fabrication methods, the flexible crystals are fabricated by using the atomic force microscopy (AFM) mechanical arm techniques. For the non-flexible crystals, they are mainly fabricated by using a self-assemble solution method and gas-phase methods such as chemical vapor deposition (CVD). Their morphology is predominantly determined by a combination of factors. The following figure presents a schematic representation categorizing these complex structures by their dimensional attributes, providing a coherent visual overview that aligns with the preceding discussion.

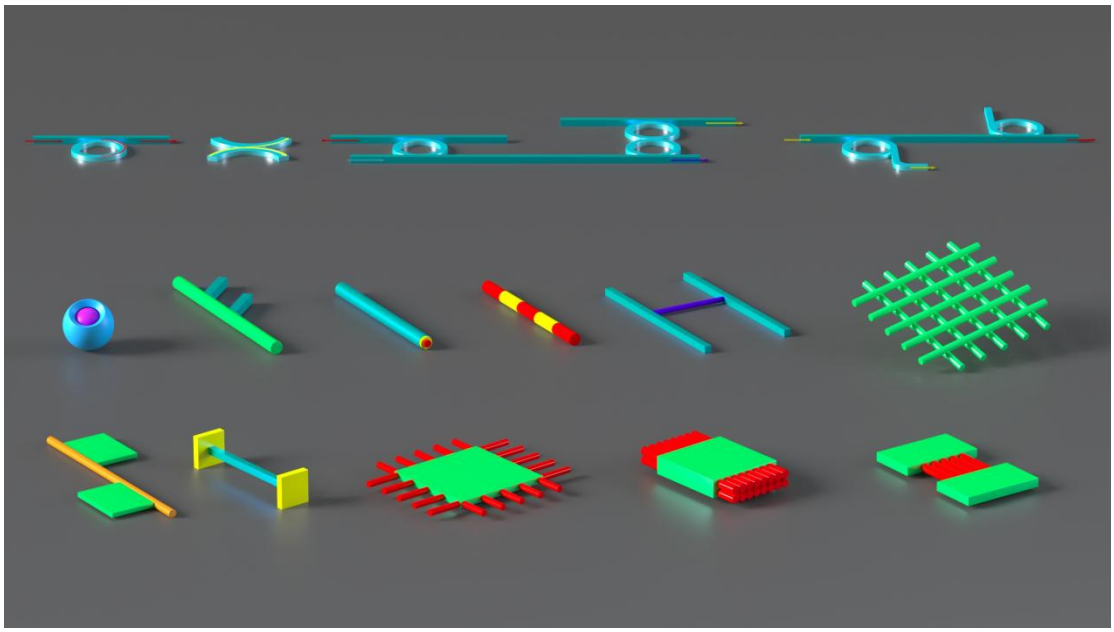

On one hand, the flexible complex structure mainly consists of two parts: a linear segment that facilitates the transmission of light, and a curved segment engineered to modify the direction of the optical output. At the junction between these two parts, ET[18] (energy transfer) particularly occur via an evanescent field coupling between two different materials, which could facilitate a change in the optical output direction of the waveguides. The organic complex structures created using NN′-bis(p-tolyl)-1458-naphthalene diimide (NDIPH) and 910-bis(phenylethynyl)anthracene (BPEA) were reported to achieve mechanically reconfigurable and optically active organic photonic integrated circuits (OPICs).[19]

On the other hand, for the non-flexible complex structure, the structures could be categorically subdivided into zero-dimensional plus zero-dimensional, one-dimensional plus one-dimensional, and one-dimensional plus two-dimensional configurations. The metal-organic framework (MOF) structures which are regarded as zero-dimensional plus zero-dimensional configurations have been extensively documented in the scientific literature. Their high specific surface area and customizable porous architecture are particularly noteworthy which position them as promising materials in applications encompassing gas storage and separation, as well as catalytic processes.[20] For the one-dimensional plus one-dimensional complex structure, mainly includes multi-block structure, core-shell structure, H-like structure, and so on. These organic complex structures exhibit diverse applications owing to their varying compositional morphologies. For example, a structure utilizing materials such as 2′2′-((1E,1′E)-1,4-phenylenebis(ethene-2,1-diyl))-dibenzenitrile (o-BCB) has been reported[21]. This structure is characterized by its unique passive/active mixed waveguide mode due to radiative energy transfer, as well as the ability to construct optical waveguides with switchable output light wavelength-bands, based on multi-block heterostructures. By altering the input ports on these heterostructures, selective outcoupling of different light wavelength bands, such as blue, blue/green, or green, is achievable, indicating their potential utility in future photonic systems.

Lastly, for the one-dimensional plus two-dimensional structure, an example includes benzo[ghi]perylene (BGP) combined with tetrafluoroterephthalonitrile (TFP) to form heterostructures has been reported.[22] It has the formation of organic topological heterostructures, which are instrumental in the advancement of integrated optoelectronics.

3. Growth Mechanism

With the rapid development of organic photonics in recent years, numerous types of organic complex structures have been reported. In this essay, the primary methodologies for fabricating organic complex structures encompass (1) the mechanophotonics approach which uses the atomic force microscope (AFM) arm to cut, bend, slice, lift and integrate the desired complex structure[23]; (2) the method based on vapor deposition and (3) self-assembly solution method. As for the mechanophotonics approach, AFM arms are capable of precisely manipulating individual crystals, and physically assembling structures as required with considerable controllability. However, it would face challenges in large-scale production and complexity of procedures. The method based on vapor deposition, it enables precise control over the thickness of the prepared materials and pure in yields[24]. Moreover, it could fabricate uniform organic complex structures[25]. While the relatively high cost and complexity of the preparation process need improvement. As for the self-assembly solution method, its main advantages are lower cost and simplicity in operation[26], but it faces challenges in achieving precise control over the complex structures and is susceptible to contamination by impurities. Overall due to its distinct nature, each fabrication method possesses inherent advantages and corresponding potential applications.

3.1 Mechanophotonics approach

The mechanophotonics approach which is fabricated through precision-driven physical manipulation, specifically use Atomic Force Microscopy (AFM) mechanical arm techniques. Due to the smooth slip planes as well as π-π interactions between crystals, AFM techniques can cut, bend, slice and integrate the crystals to obtain the desired complex structure. Professor Chandrasekar's team has done extensive work in this field. One example is their research on complex structures which is formed by bending the DPIN crystal to a circle and integrated it with CPIN crystal (shown in figure 1a). By forming the μ-OPIC with DPIN and CPIN, the wavelength of the transmitted light changes at the connecting junction due to the energy transfer principle, specifically, between orange and green in this complex structure. Moreover, it is capable of performing mechanism-selective and direction-specific light output based on the electronic properties of the crystal and the position of the input signal (shown in figure d-h)[27]. Similarly, as shown in Figure 2e-g, another type of complex structure is formed by connecting the 2-((E)-(6-methylpyridin-2-ylimino)methyl)-4-chlorophenol (SB1) crystal and the 2-((E)-(6-Bromopyridin-2-ylimino)methyl)-4-bromophenol (SB3) crystal end-to-end. It would firstly bend the SB3 and connected it to the SB1 where tip-to-tip coupling could be notice at the connection. This AFM-constructed "j-shaped" organic complex structure realizes input-selective by means of active and passive waveguide principles, re-absorption mechanisms.[28]
Another example is the OPIC which is formed by using BPEA (910-

bis(phenylethynyl)anthracene) and NDIPH(NN'-bis(p-tolyl)-1458-naphthalenediimide). The fabrication of this OPIC is mainly made by 2 steps 1) Bending the NDIPH into a ring structure and 2) integrate it with the BPEA by using the AFM techniques. The fabricated OPIC-II could change the direction from x-axis to y-axis. Moreover, the OPIC further bends the NDIPH, thereby changing the direction of terminal 1. In this way, the OPIC can achieve directed output of light signals and further demonstrate its mechanical compliance and structural reconfigurability. The figure k_1-k_4 displayed the various 1 input terminal and 3 output terminals.

In addition to the OPIC that composed of two organic materials, an organic crystal multiplexer has been reported which is made up of three types of organic flexible crystals and could be used for visible light signal transportation. The wavelength division multiplexer (WDM)[29] which made of DBA, BPP and $BTD2CF_3$ is constructed by using the AFM(figure l-m). The Crystals made up of three different materials emit light at different wavelengths (λ1, λ2 and λ3). Through the resonant energy transfer mechanism, light energy can be transferred between the crystals. This mechanism allows one crystal emit its own light and as well as trigger other crystals to emit light at the same time, thus allowing light to be emitted without external excitation. In this way, a single input signal can be converted into a composite output signal containing three different light wavelengths (λ1+λ2+λ3). This enables the multiplexer to efficiently transmit and extend the bandwidth of optical signals, making it ideally suited for use in efficient optical communications and information processing applications (shown in figure n-o).

In conclusion, the mechanophotonics approach which leverage precision-driven Atomic Force Microscopy (AFM) techniques could effectively fabricate complex structures by manipulating organic crystals with high precision. This method not only enables the creation of intricate and reconfigurable photonic structures but also enhances the performance and versatility of optical devices through controlled energy transfer and selective light output. Consequently, mechanophotonics approach offers significant potential for advancements in optical communications and information processing, paving the way for innovative applications in these fields.

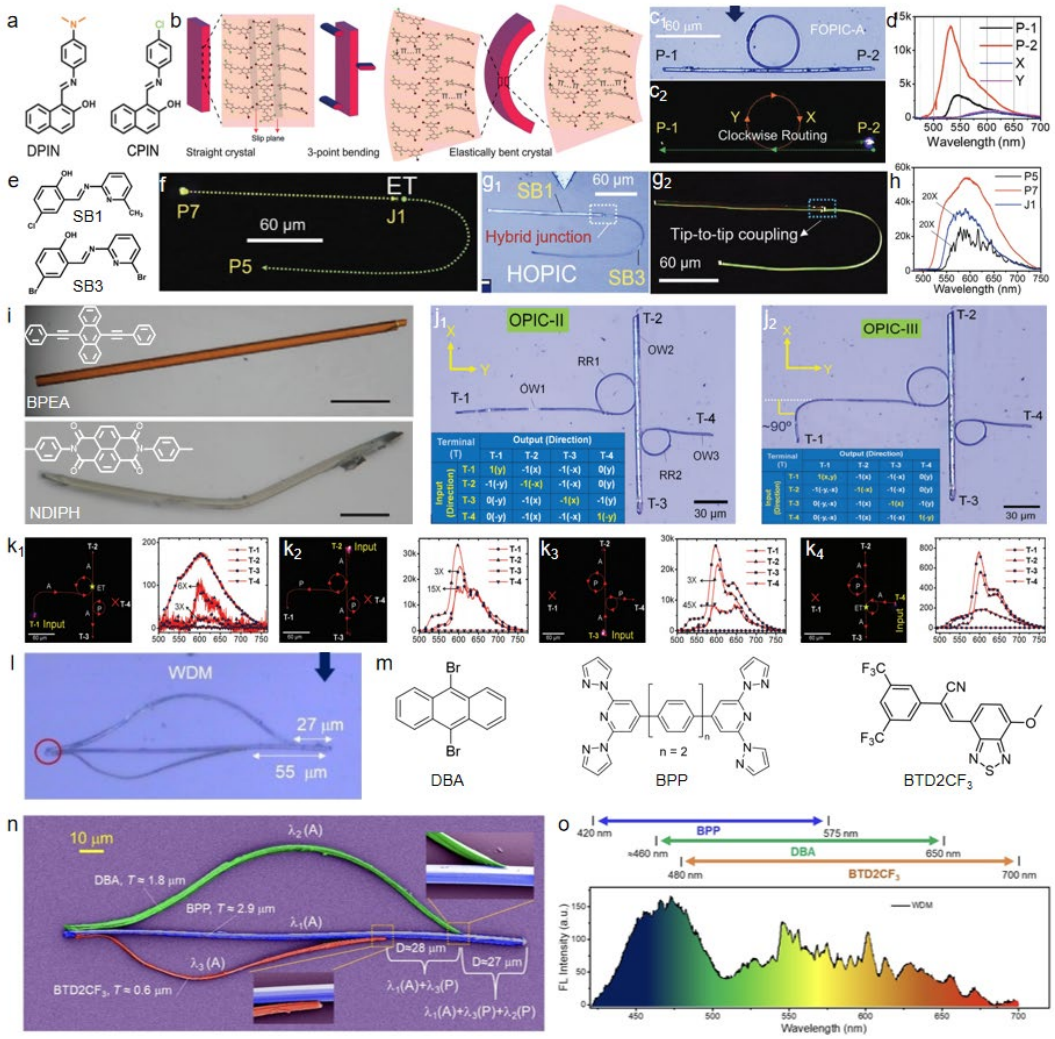

Figure 1. (a)

3.2 Solution-based self-assembly approach

The solution-based self-assembly approach primarily relies on the regulation of non-covalent interactions between molecules for the large-scale production of desired materials. This method has several advantages including 1) more cost-effective 2) involves fewer steps and simpler to operate. 3) suitable for growing large-size crystals. Herein, this method has been widely applied for growing organic complex structure such as core-shell structure[30], heterostructure[31] and so on. One case of precise, solution-based, layered self-assembly was reported by use 4,4'-((1E,1'E)-(2,5-dimethoxy-1,4-phenylene)bis(ethene-2,1-diyl))dipyridine (DPEpe) , 1,4-diiodotetrafluorobenzene (F4DIB) and 4-bromo-2,3,5,6-tetra-fluorobenzoic acid (BrFTA)[32]. The growth of the complex structure could be divided in 2 stages (Figure 3a). In the first satge, DPEpe respectively forms eutectic with F4DIB and BrFTA to obtain green eutectic DPEpe-F4DIB and red eutectic DPEpe-BrFTA under UV-band excitation. In the second stage, DPEpe-F4DIB eutectic was epitaxially grown on the tip or side surface of DPEpe-BrFTA nanowires to obtain the complex structure. Notably, the length ratio of the dPEpe-BrFTA co-crystal at the center of the three nanowires shows a linear relationship with the ratio of BrFTA to DPEpe

(Figure 3b_1-b_3). By adjusting the formation of hydrogen/halogen bonds during the layer-by-layer self-assembly process in LG, the length of the DPEpe-F4DIB or DPEpe-BrFTA co-crystals in TWNs can be quantitatively controlled, thereby enabling customization at the microscopic level of complex structures (Figure 3c_1-c_2).

Another solution-based example of complex structure is the "H"-like nanowire heterostructures which is facilitated by the cooperative assembly of molecules 2,4,5-triphenylimidazole (TPI) and 2-acetyl-6-dimethylamino-naphthalene (ADN) (Figure 3d)[33]. After adding 80°C water as the poor solvent in the 100 μL THF mixture with TPI and ADN. The TPI nanowires are formed firstly and then the ends of the growth line serve as site-specific nucleation centers for the heterogeneous epitaxial growth of ADN nanowires, thereby forming a unique "H" complex structure with two parallel ADN nanowires bridged vertexically 90 degree by one TPI nanowire (Figure e). Specifically, figure 2f presents a standard transmission electron microscopy (TEM) image of the junction area within an “H”-like nanowire heterostructure, illustrating that the nanowires composed of TPI and ADN display uniform morphologies and smooth surface. A focused laser beams excited 3 part of the "H" like complex structure (351 nm, Figure 3g) and the corresponding spatially resolved microarea PL spectra were revealed in Figure 3h. For region 1 and 3, the PL spectra which indicates the maximum emission at 450 nm is regarded as the AND. For region 2, the peak is centered at 405 nm which represents TPI. Herein, the bridge of “H”-like organic complex structure is constructed by TPI, while the two parallel nanowires are formed from ADN molecules.

Except 1D complex structure, 2D complex which consists of 1D microbelts/microwires as well as 2D microplates has also been reported[34]. There are 2 stages included in the growth process. Due to DFT calculation of the π−π interaction intensity (E_o-BCB = −25.56 kcal mol−1, E_m-BCB = −15.49 kcal mol−1, E_{TPBe} = −5.06 kcal mol−1), firstly, the self-assembly process in the solution forms microbelts using o-BCB (1,4-phenylenebis(ethene-2,1-diyl)dibenzonitrile), 1D microwires using m-BCB (1,4-dimethoxy-2,5-di(E)-bis(2-methylstyryl)benzene). Secondly, 2D microplates TPBe (2,5,8,11-tetra-tert-butylperylene) will grow epitaxially on the 1D microbelts/microwires to form two types of complex 2D structures(shown in figure 3i). By using PL emission characterization, it can be further verified that the trunck and branches of the complex structure respectively correspond to m-BCB microwires and TPBe microplates.

In summary, the solution-based self-assembly approach offers significant advantages due to its cost-effectiveness, ease of implementation, and ability to grow large-size crystals[35-37]. The simplicity of this method lies in its straightforward process, which typically requires only basic laboratory equipment and avoids the need for high-temperature conditions or complex fabrication techniques. This method leverages non-covalent interactions to facilitate the large-scale production of complex organic structures. It is particularly effective in creating intricate architectures like core-shell and heterostructures and so on. These examples illustrate the method's capability to produce intricate and customizable microstructures.

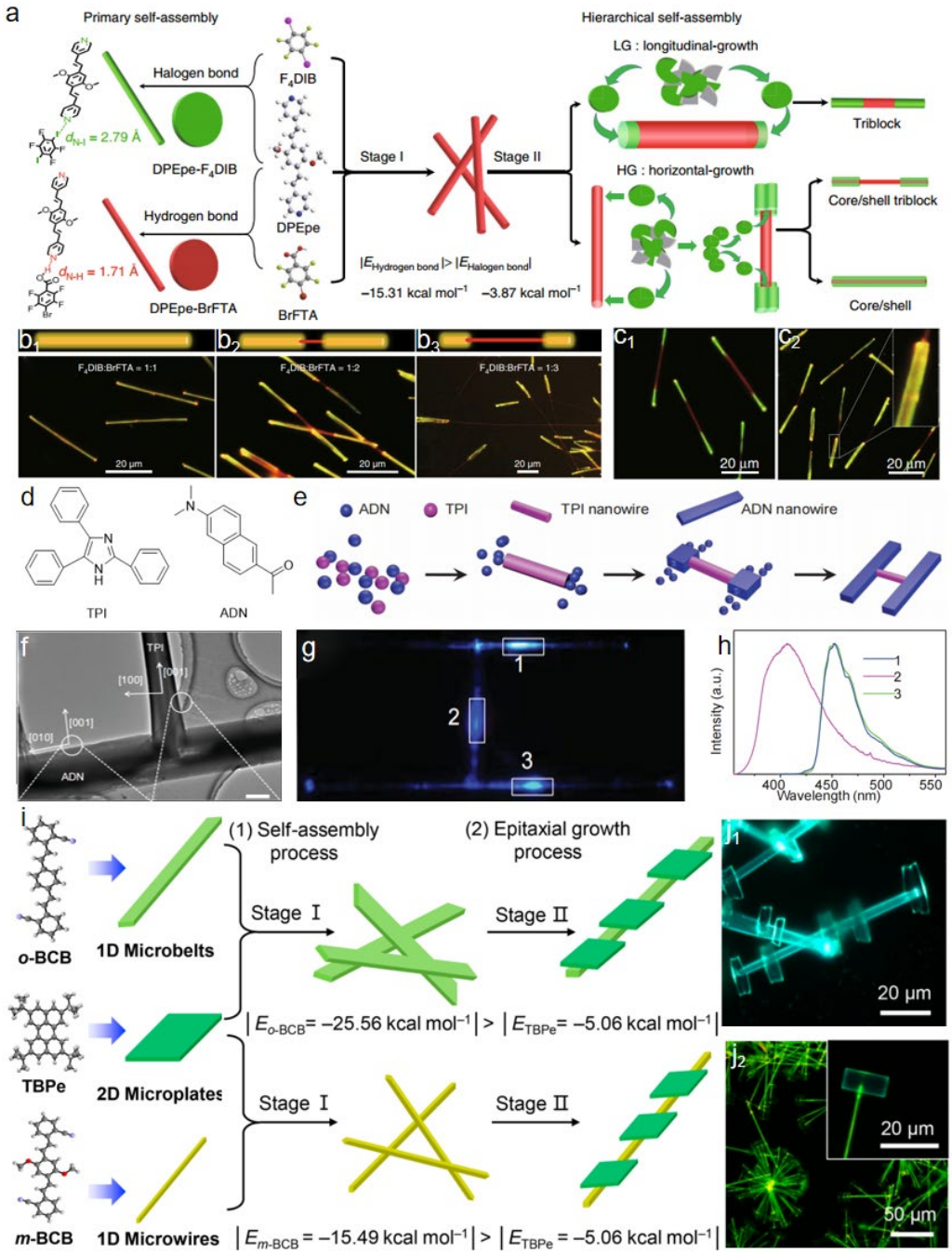

3.3 Vapor based approach

The approach based on vapor deposition mainly consists of physical vapor deposition[38], chemical vapor deposition[39], microspacing in-air sublimation[40] and so on. This approach has been gaining increasing attention due to the complex structure created by this method has several advantages including: 1）Exhibiting excellent photonic and optoelectronic properties such as high quantum yield, low waveguide loss, and high quantum mobility.[41] 2）Allowing more direct control over deposition rate and sequence, resulting in higher quality crystals. 3）Reducing impurities since it is contamination-free. One example of the complex structure with excellent morphology which fabricated by the usage of Vapor based approach is using the

dicyanomethylene-2-methyl-6-(p-dimethylaminostyryl) 4H-pyran (DCM) and perylene.[42] The growing process of DCM/perylene is shown in Figure 4a. Firstly, DCM micro-rods are grown on the substrate as the backbone at 175°C, and then perylene a-micro-squares are selectively grown on the DCM at 135°C. This selective growth occurs at ambient pressure, where the specific growth conditions allow the formation of well-defined heterostructures without the presence of unwanted thin films or defects (shown in Figure 2b). The DCM single crystal, perylene single crystal, as well as the DCM/perylene complex structure grown using the vapor phase growth method, exhibit much better morphology compared to those grown using acetonitrile (HPLC grade) in a solution-based self-assembly approach. This underscores the advantages of this method in enhancing crystal quality, particularly in achieving smoother surfaces and more precise structures, while effectively avoiding the defects commonly observed in solution-based methods.

Another example which uses Physical Vapor Transport (PVT) Technique to construct the multi-block complex structure is using the Dicyanomethylene-2-methyl-6-(p-dimethylaminostyryl) 4H-pyran (DCA) and Perylene (Pe).[43] The formation of the DCA/Pe complex structure is driven by a charge-transfer (CT) interaction,[44] resulting in the assembly of multiblock microrods with alternating blocks of DCA and Pe (shown in figure e). In this context, the PL spectra indicate that the triblock heterostructures exhibit distinct emission bands for green-emitting A and red-emitting Pe-A complexes. The PXRD patterns confirm that these microrods maintain their intrinsic crystal structures and photoluminescent properties, regardless of the growth sequence of A or B domains (shown in figure f). As a result, the FM images (Figures g_1- g_6) displays some different types multiblock complex structure of FM images, demonstrating the versatility and precision of the vapor phase growth method in fabricating complex structures.

Additionally, a two-step vapor-phase growth process for creating dendritic organic heterojunctions which composed of aluminum tris(8-hydroxyquinoline) (Alq_3) microwire trunks and 1,5-diaminoanthraquinone (DAAQ) nanowire branches has been reported (figure i)[45]. Firstly, Alq_3 microwires are synthesized as the primary trunk structure through a liquid-phase self-assembly method (shown in figure h). Subsequently, DAAQ nanowires are epitaxially grown on the Alq3 microwires using a physical vapor deposition technique, forming branched structures. The process setup involves heating DAAQ powder in an oil bath while nitrogen gas transports the vaporized molecules to the substrate, where selective nucleation occurs at the surfaces of the Alq3 microwires. The SEM images (k1 to k4) show the progressive growth of DAAQ nanowires on Alq3 microwires at various time points (0 min, 2 min, 4 min, and 6 min), demonstrating the formation of the dendritic heterostructures (figure j). This method allows precise control over the spatial arrangement and density of the nanowire branches, resulting in complex, well-defined heterojunctions suitable for advanced photonic applications.

In conclusion, the vapor deposition approach effectively fabricates complex structures with high precision[46], offering advantages such as excellent photonic and optoelectronic properties, precise control over deposition rates, and reduced contamination. This method effectively highlights its capability to reliably produce well-defined heterojunctions with intricate and complex morphologies, making it highly suitable for advanced material applications.

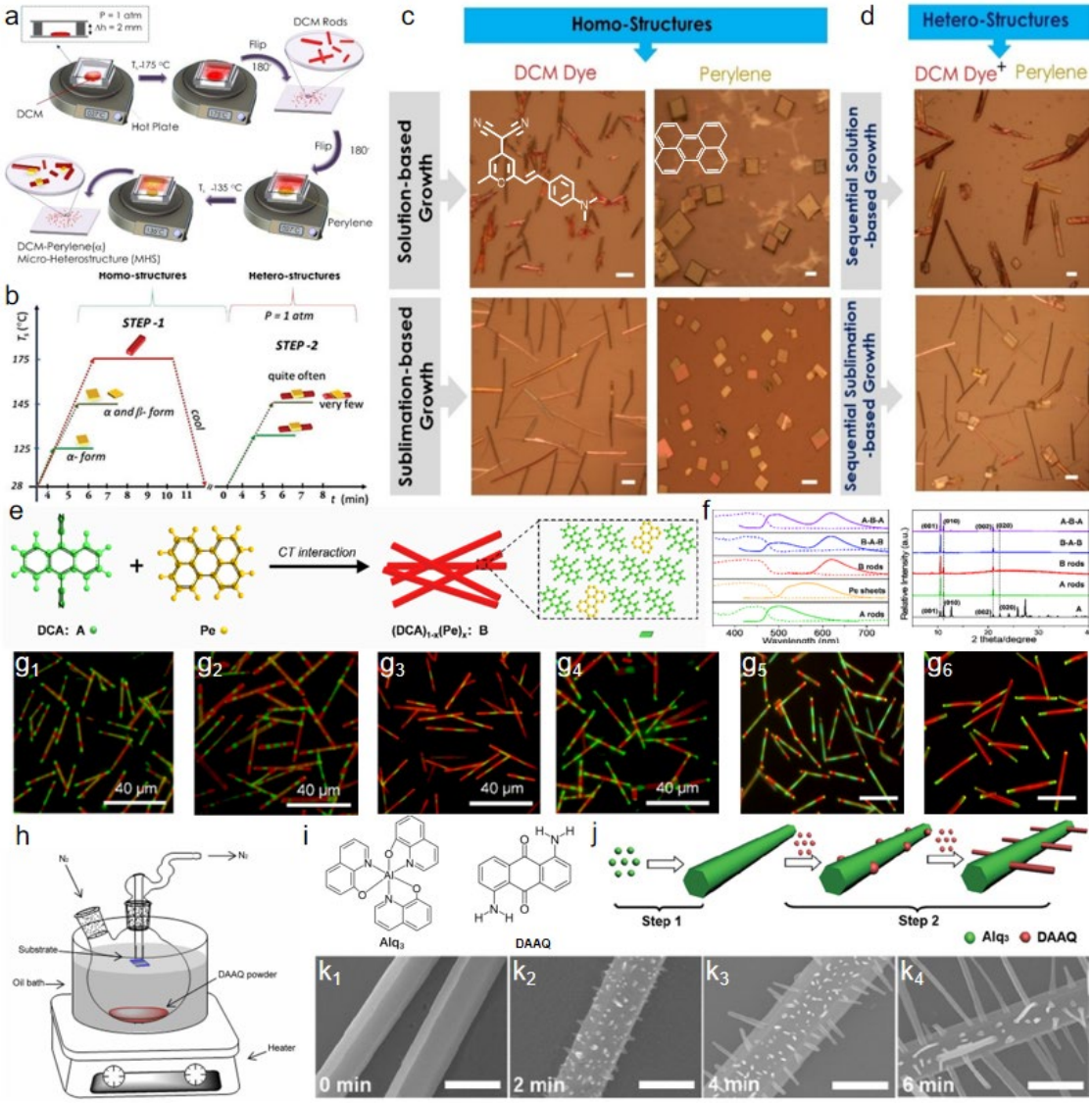

4. Application

Organic complex structures have gained increasing importance in recent years due to the rapid development of modern technology. As a material system with high designability and diversity, organic complex structures not only enable precise functional control in various ways but also offer significant advantages such as low cost[47], easy processing, light weight[48], and flexibility[49]. Through chemical synthesis methods, scientists can design organic molecules with specific functions and structures to meet various application requirements. Their diversity and tunability provide a broad space for the realization of innovative technologies. In this context, we will explore the significant advancements and applications of complex structures in the following fields: 1) optical logic gates[50] and 2) optical anti-counterfeiting[51].

4.1 Logic gate

Optical logic gates have drawn much attention due to their high speed and low energy consumption for potential applications such as photonic chips, high-speed optical computing,

and advanced communication systems. To realize the optical logic gate application, significant progress has been made in the development of materials and designs that can efficiently manipulate light at the nanoscale, enabling faster and more efficient information processing. A chip-like organic complex structure composed of benzo[ghi]perylene (BGP) microsheets and BGP/3,4,5,6-tetrafluorophthalonitrile (o-TFP) cocrystal microrods has been reported recently[52]. These structures exhibit significant optical properties, particularly suitable for optical logic gate applications. By changing the excitation position, the spatial distribution and intensity variation of the optical signals can be observed (Figure a2-c2), along with the relative optical intensity at the output terminals (Figure a3-c3). BGP microsheets would achieve multi-terminal optical signal output and modulation if excitation position has changed. Different excitation positions result in varying optical intensities at the output terminals. By adjusting the excitation light position, the on/off state of different terminals can be controlled, achieving digital signal encoding (shown in figure d). Herein, this chip-like organic heterostructure, combining the optical properties of BGP microsheets and BGP/o-TFP cocrystal microrods, can achieve multi-terminal optical signal output and modulation, making it highly suitable for constructing efficient optical logic gates. Beyond the advancements in BGP-based structures, complex structure which has multi-channels and multi-waveguide modes has been realized and reported[27]. By altering the input terminal of μ-OPIC, the multi-channel outputs will correspondingly exhibit specific changes (Figure f1-f4), as well as the relative optical mode at the output terminals. The DPIN and BPIN microcrystals can achieve multi-terminal optical signal output and modulation with different excitation positions, leading to varying optical intensities at the output terminals. By adjusting the excitation light position, the states of different terminals can be controlled (shown in figure e). Therefore, the μ-OPICs which combine the optical properties of DPIN and BPIN microcrystals, can achieve specific logic input and output, making them highly suitable for the usage of optical logic gates.

Another study demonstrated the growth and optical properties of dendritic organic heterojunctions composed of Alq_3 microwires and DAAQ nanowire branches[45]. SEM images (Figures g_1 and g_2) indicate the DAAQ nanowires grown vertically on Alq3 microwires. The experimental setup (Figure h) involved focusing a laser on different input points of the Alq_3 microwires and adjusting the incident angle (θ) to observe changes in optical signal distribution and intensity.

The results (Figure i) revealed that the spatial distribution and intensity of the optical signals varied with different incident angles. By measuring the PL decay curves at various positions within the complex structure and utilizing the polarization characteristics of light to modulate the output signals from the branch channels, it was observed that the PL intensity exhibited a sinusoidal modulation with a 180° period as a function of the polarization angle (θ). The maximum and minimum PL intensities occurred at $\theta = 15°$ and $\theta = 105°$, respectively, indicating the preferred direction of π-conjugated alignment in the Alq3 crystalline trunk. Moreover, the on/off ratio of the maximum to minimum emission intensity was determined to be 6.7, and the polarization ratio (ρ) was 0.74, surpassing previously reported values for conjugated polymer and inorganic semiconductor nanowires. By controlling the incident light polarization, it is

possible to specifically modulate light propagation within the complex structure. These findings suggest that it holds significant potential for applications in optical signal switches.

Lastly, the complex structure formed using 2,4,5-Triphenylimidazole (TPI) and 1,4-Dimethoxy-2,5-di[4'-(cyano)styryl]benzene (COPV) as backbones and branches respectively, has been reported (shown in Figures j and k)[53]. Similarly, by using polarized excitation microscopy (Figure l), it was observed that the emission intensity from the 1,4-Dimethoxy-2,5-di[4'-(cyano)styryl]benzene (COPV) microribbon and 2,4,5-Triphenylimidazole (TPI) complex structure varied periodically with the polarization angle. Specifically, θ = 20 or 200° corresponds to the laser polarization being parallel to the transition dipole moment of COPV molecules, resulting in maximum emission (ON state), while θ = 110 or 290° corresponds to perpendicular polarization, resulting in minimum emission (OFF state). This modulation of emission intensity demonstrates the COPV-TPI complex structure as a multichannel optical router with high on/off ratios and polarization ratios (Figure m), indicating potential applications in advanced photonic circuits and optical communication systems.

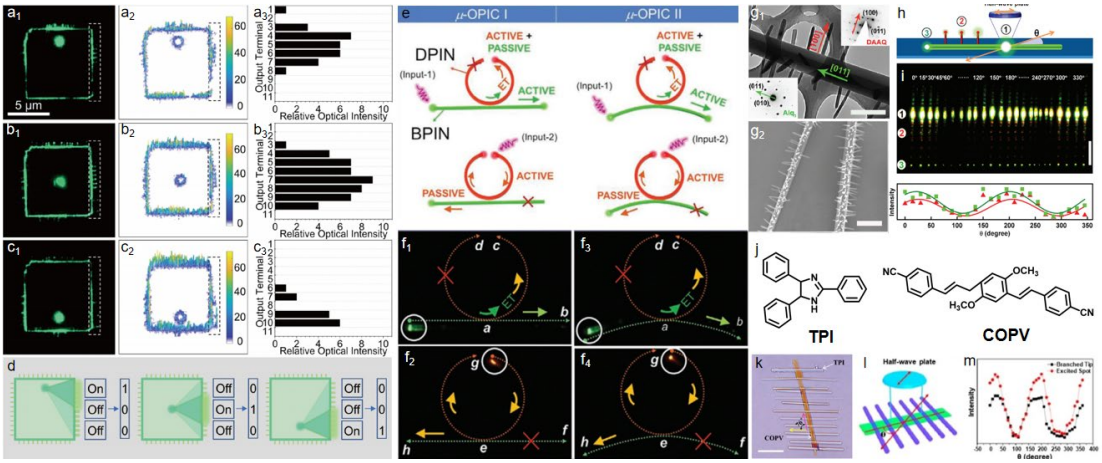

4.2 Optical anti-counterfeiting

Optical anti-counterfeiting technologies have become increasingly important due to the growing need for high security and cost-effective solutions in various fields, including secure identification, advanced packaging and so on. The rise in sophisticated forgery techniques has necessitated the development of more advanced anti-counterfeiting measures. By exploiting the unique properties of light manipulation at the nanoscale, researchers have made significant progress in creating materials and designs that offer robust and easily verifiable security features. These optical technologies not only enhance the protection against forgery and unauthorized duplication but also provide a versatile platform for integrating additional security measures, such as holograms, color-shifting inks, and photonic crystals, making them indispensable in the fight against counterfeiting. For example, a multi-material organic micro/nano heterostructure system was reported, exhibiting notable optical properties ideal for anti-counterfeiting[35]. These heterostructures which formed through the co-assembly of fluorescent molecules (BPEA) and phosphorescent molecules (MCzT), could be adjusted to have branched structures with either fluorescent or phosphorescent molecular backbones. By using the time-resolved luminescence of this complex structure, the first level of anti-counterfeiting can be achieved. By alternately switching the excitation source, the luminescence of the backbone and branch nanostructures changes accordingly. As shown in

Figure 4a, after the UV light is turned off, the luminescence of the backbone disappears immediately, while the branches display persistent phosphorescence for several seconds. Additionally, excitation-dependent luminescence can be utilized to achieve the second level of anti-counterfeiting. When the excitation light is switched from UV to green, the color of the branches change from blue to red (Figure b). Figures c and d demonstrate the luminescence characteristics caused by switching different wavelength light sources, thereby achieving and applying optical dual anti-counterfeiting.

Another example that uses responsive metal-organic frameworks (MOFs) with epitaxial growth techniques has been reported[54]. Figure e illustrates the concept of decoding covert photonic barcodes under external stimuli, where the barcode's color changes and becomes readable only under specific conditions. To obtain an ideal anti-counterfeiting structure, 0D+1D MOF heterostructures were synthesized (Figure f). This process starts with a MOF block containing 2% Eu as a precursor and results in a heterostructure with 5% Eu in the end blocks and 2% Eu in the central block. Figures g1 and g2 depict the responsive MOFs under different temperatures, showing a color change from 298 K to 350 K, which is utilized for encoding information. In the practical application of these MOFs in a packaging scenario, the barcodes on the packaging are initially invisible (figures h1-h2). Herein, the decoded barcodes could be realised and providing double insurance: Barcode-1 is decoded under normal conditions, while Barcode-2 requires the elevated temperature to reveal the hidden information, ensuring a higher level of security and authenticity (figures i_1-i_2).

Finally, the multiblock complex structure formed by [Ir(ppy)2(pzpy)] and [Ru(bpy)3]2 has been reported (Figures j)[55]. Under UV irradiation, these multiblock complex structures exhibit a gradient of green-red-yellow emissions along their length (Figure k). While the excitation wavelength shifts to the visible range (around 550 nm), the red segments maintain their emission properties. In contrast, the original green tips become non-emissive and the middle part emits weakly (Figure l). By employing laser confocal fluorescence microscopy, the photoluminescence intensities at various positions along the single heterojunction rod were treated as spectroscopic encoding information (figure m-n). As shown in Figure o, the heterojunction rod is illuminated at two different excitation wavelengths, leading to distinct emission modes. These emission patterns create significant optical contrast along different parts of the rod. The emission intensity at each position is encoded as "0" or "1", providing a basis for advanced photonic signal processing. Figure p displays the result of this optical encoding, where the emission intensities at different positions are sensitively mapped and decoded, forming a system of spectroscopic encoding information.

In essence, these multicolor emissive nanorods provide interesting coding/decoding functions at the nanoscale by utilizing different excitation wavelengths as encryption keys and defined patterns of emission intensity as output signals. This capability underscores the potential of these nanorods for advanced applications in secure communications and complex biological assays.

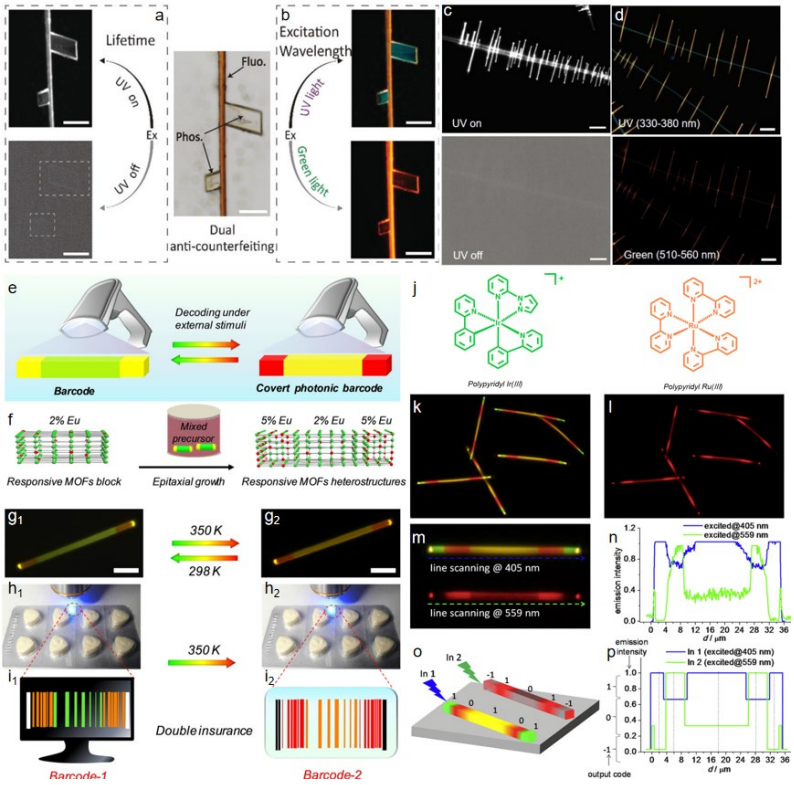

5. 展望

Compared to single-structure/inorganic materials, organic materials offer significant advantages in various aspects, such as enhanced flexibility in modifying molecular structures, multitude of structures and optoelectronic properties, and tunable optoelectronic properties. These attributes make them highly suitable for advanced applications in optoelectronics and photonic devices. In this review, we categorized organic complex structures based on their dimensional attributes and discussed three fundamental methods (mechanophotonics, solution-based self-assembly, and vapor-based approaches) that used in the fabrication of complex structures.

However, the fabrication of organic complex structure is susceptible to environmental factors like temperature, humidity, pressure, solution concentration and so on. Additionally, the influence of weak intermolecular forces (such as van der Waals forces,[56] π–π interactions, [57-60]hydrogen bonds,[61-63]and halogen bonds[64-66]) renders the controllable growth process of organic micro/nanocrystals significantly more complex, making controlled and large-scale production for application still a significant challenge in industry. Beyond the challenges in fabrication, several other critical issues and obstacles need to be addressed. The stability and performance consistency of organic micro/nanocrystals under operational conditions are major concerns. The combination of different materials involves complex epitaxial relationships, which are crucial for the precise construction of organic complex structure. This complexity introduces significant obstacles in ensuring the reliability and reproducibility of the final

products. Additionally, integrating these complex structures into existing manufacturing processes without compromising their optoelectronic properties remains a daunting challenge. Overcoming these problems is essential for achieving controlled and large-scale production for practical applications in the industry.

In summary, great progress has been made in this field, with significant advancements in the design, synthesis, and application of organic complex structures. Researchers have successfully demonstrated various applications in optoelectronics, photonic integrated circuits, and optical anti-counterfeiting. However, in order to fully realize the potential of complex structure, it is essential to develop new types of complex structures to achieve desirable performance.

Table (按照时间发展顺序和 0+1，1+2 的总结)

Structure	Component		Years	Method	Application	Ref
Flexible	(E)-1-(4-(dimethylamino)phenyl)iminomethyl-2-hydroxyl-naphthalene (DPIN)		2018	Micromechanical manipulation	Organic optical waveguides	
	3,4-dimethyl-4-(dimethylamino)azobenzene (DDAB)		2019	Micromechanical manipulation	Passive waveguide, photo-actuator	
	2,5-bis({2-hydroxyethyl}amino)-terephthalate (BEAT)		2019	Micromechanical manipulation	Organic optical waveguides	
	2,5-diaminoterephthalate (DMDAT)		2019	Micromechanical manipulation	Active waveguide	
	(Z)-4-(1-cyano-2-(4-(dimethylamino)phenyl)vinyl) benzonitrile (CN-DPVB)		2020	Micromechanical manipulation	Active waveguide	
	Dithieno[3,2-a:2',3'-c]phenazine (SYN)		2020	Micromechanical manipulation	Active waveguide, WDM, optical circuit	
	9,10-bis(phenylethynyl)anthracene (BPEA)	N,N'-bis(p-tolyl)-1,4,5,8-naphthalenediimide (NDIPH)	2021	Micromechanical manipulation	All-organic photonic integrated circuits by micromanipulation of organic crystals	
	(E)-1-(4-bromo)iminomethyl-2-hydroxyl-naphthalene (BPIN)	(E)-1-(4-(dimethylamino)-phenyl)imino methyl-2-hydroxyl-naphthalene (DPIN)	2021	Micromechanical manipulation	Organic optical waveguides	
	2-({(E)-(6-methylpyridin-2-ylimino) methyl)-4-chlorophenol (SB1)	2-({(E)-(6-Bromopyridin-2-ylimino) methyl)-4-bromophenol (SB3)	2022	Mechanophotonics approach	Optical signal processing	
Core-shell	Trinitrofluorenone (TNF)	Hexabenzocoronene (HBC) amphiphile	2006	Sequential Self-assembly	-	
	Iridium(III) bis(2-phenylbenzothiozolatoN,C$^{2'}$) ((BT)2Ir(acac))	Perylene	2010	Microemulsion-assisted chemical reaction method	White light emission	
	9,10-bis(phenylethynyl) anthracene (BPEA)	Bis(2,4,5-trichloro-6-carbopen-toxy-phenyl) oxalate (CPPO)	2012	Sequential self-assembly	Hydrogen PeroxideVapor Sensing	
	Copper phthalocyanine (CuPc)	5,10,15,20-tetra(4-pyridyl)-porphyrin (H2TPyP)	2012	Physical vapor transport(PVT) technique	Photodiodes;Photoswitch;Photovoltaic	
	P3HT:PCBM	Polyvinylpyrrolidone (PVP)	2015	Electrospinning	Coaxial electrospinning	
	Polystyrene (PS)	Poly(methylmethacrylate) (PMMA)	2017	Electrospinning	Coaxial electrospinning	
	4,4'-((1E,10E)-(2,5-dimethoxy-1,4-phenylene) bis-(ethene-2,1-diyl))dipyridine (DPEpe)	4,4'-((1E,10E)-(2,5-dimethoxy-1,4-phenylene)bis -(ethene-2,1-diyl))dipyridine –HCl (DPEpe-HCl)	2019	Stepwise seeded growth	Optical waveguides	
	BSA	Glycerin	2019	Inkjet printing	Full-color laser displays	
	Polystyrene (PS)	BSA	2020	Inkjet printing	Full-color laser displays	
	Dibenzothiophene-1,2,4,5-tetracyano benzene (S-TCNB)	Fluorene-TCNB (C-TCNB)	2020	Solution-phase epitaxial growth	Stepwise seeded growth	
	Dibenzothiophene-1,2,4,5-tetracyano benzene (S-TCNB)	Carbazole-TCNB (N-TCNB)	2020	Solution-phase epitaxial growth	Stepwise seeded growth	
	Fluorene-TCNB (C-TCNB)	Carbazole-TCNB (N-TCNB)	2020	Solution-phase epitaxial growth	Stepwise seeded growth	
	Dibenzo[g,p]chrysene (DgpC)Tetrafluoroterephthalonitrile (TFP)1,2,4,5-tetracyan obenzene (TCNB)		2021	Sequential self-assembly	White light emission	
Branch	4,4'-bis(phenylethynyl)anthracene (BPEA)	Ag	2012	Direct site-selected growth	All-optical modulator	
	Tris-(8-hydroxyquinoline)aluminum (Alq3)	Polystyrene (PS)	2015	Emulsion-solvent-evaporation method	WGM laser	
	coronene	perylene	2016	Solution assembly strategy	-	
	dye-doped polystyrene	Ag	2017	capillary force-assistedemulsion assembly method	multicolorsubwavelength laser	
	Tris-(8-hydroxyquinoline)aluminum (Alq3)	(phenylethynyl)anthracene (BPEA)	2019	sequential self-assembly	-	
	1,4-dimethoxy-2,5-di(E)-bis(2-methylstyryl) benzene (m-BCB)	2,5,8,11-tetra-tert-butylperylene (TPBe)	2020	Sequential self-assembly approach	Nanoscale optical coding/decoding functions	
	2,2'-((1E,1E')-1,4-plenylenebis(ethene-2,1 diyl))-dibenzonitride (o-BCB)					
	benzo[ghi]perylene (BGP)	tetrafluoroterephthalonitrile (TFP)	2020	hierarchical self-assembly	photonic transistor	
	benzo[ghi]perylene (BGP)	octafluoronaphthalene (OFN)	2020	hierarchical self-assembly	photonic transistor	
	3,3'-((1E,1'E)-anthracene-9,10-diylbis(ethane-2,1-diyl))dibenzonitril (m-B2BCB)		2021	solvent-evaporation method	optical waveguides	
	Benzo[ghi]perylene (BGP)	3,4,5,6-tetrafluorophthalonitrile(o-TFP)	2023	Sequential self-assembly	Optical signal processing	
Multiblock	2,4,5-triphenylimidazole (TPI)	Iridium(III) bis(2-phenyl benzothiozolato N,C2') ((BT)2Ir(acac))	2012	Doping method	Optical waveguides	
	2,4,5-triphenylimidazole (TPI)	9,10-bis (phenylethynyl) anthracene (BPEA)	2012	Doping method	Optical waveguides	
	2,4,5-triphenylimidazole (TPI)	3-(2-benzothiazoly)-7-diethylaminocoumarin(Coumarin 6)	2013	Doping method	photonic diodes; photonic transistor	
	4,4'-(4,4'-(perfluorocyclopent-1-ene-1,2-diyl) bis(5-methylthiophene-4,2 diyl))bis(ethyne-2,1-diyl)bis(2,6-di(1H-pyrazol-1-yl)pyridine) (BPP-THIO-Lo)	4,4'-(4,4'-(perfluorocyclopent-1ene-1,2-diyl)bis(5-methylthiophene-4,2-diyl))bis (ethyne-2,1-diyl)bis(2,6-di(1H-pyrazol-1-yl) pyridine) (BPP-THIO-Lc)	2015	photochromic method	optical waveguides	
	1,4-bis(a-cyano-4-diphenyl)-2,5-diphenyl benzene (OPV-D)	1,4-bis(a-cyano-4-diphenylaminostyryl) -2,5-diphenylbenzene (OPV-A)	2018	liquid-phase co-assemblymethod	photonic transistors	
	[Ir(ppy)2(pzpy)]+ (ppy = 2-phenylpyridine, pzpy = 2-(1H- pyrazol-1-yl)pyridine)	[Ru(bpy)3]2+ (bpy = 2,2'-bipyridine)	2018	Doping method	Optical logic gate;ncoding/decoding	
	1,3,5-benzenetricarboxylic acid (BTC)	Lanthanide (Ln) ions	2019	Stepwise epitaxial growth	Barcodes	
	Tri-phenylene	Perylene	2019	Stepwise epitaxial growth	Optical logic gate	
	Trans-2,2'-((1E,1'E)-1,4-phenylenebis (ethene-2,1-diyl))-dibenzonitrile	Cis-2,2'-((1E,1'E)-1,4-phenylenebis (ethene-2,1-diyl))-dibenzonitrile	2019	Photochromic method	Optical logic gate	
	4,4'-((1E,1'E)-(2,5-dimethoxy-1,4-phenylene)bis(ethene-2,1-diyl))dipyridine (DPEpe)		2019	Hierarchical self-assembly	Optical logic gate	
	4-bromo-2,3,5,6-tetra-fluorobenzoicacid (BrFTA)1,4-diiodotetra-fluorobenzene (F4DIB)					
	Benzo[ghi]perylene-1,2,4,5-tetracyanobenzene(BTB) benzo[ghi]perylene	Tetrafluoroterephthalonitrile (BTP)	2021	Hierarchical self-assembly	Optical logic gate	

图 67-72

(1) Tsumura, A.; Koezuka, H.; Ando, T. Macromolecular electronic device: Field-effect transistor with a polythiophene thin film. *Applied Physics Letters* **1986**, *49* (18), 1210-1212. DOI: 10.1063/1.97417.
(2) Deng, W.; Lv, Y.; Zhang, X.; Fang, X.; Lu, B.; Lu, Z.; Jie, J. High-resolution patterning of organic semiconductor single crystal arrays for high-integration organic field-effect transistors. *Materials Today* **2020**, *40*, 82-90. DOI: 10.1016/j.mattod.2020.06.004.
(3) Yang, F.; Sun, L.; Han, J.; Li, B.; Yu, X.; Zhang, X.; Ren, X.; Hu, W. Low-Voltage Organic Single-Crystal Field-Effect Transistor with Steep Subthreshold Slope. *ACS Appl Mater Interfaces* **2018**, *10* (31), 25871-25877. DOI: 10.1021/acsami.7b16658 From NLM PubMed-not-MEDLINE.
(4) Qiao, C.; Zhang, C.; Zhou, Z.; Yao, J.; Zhao, Y. S. An Optically Reconfigurable Förster Resonance Energy Transfer Process for Broadband Switchable Organic Single-Mode Microlasers. *CCS Chemistry* **2022**, *4* (1), 250-258. DOI: 10.31635/ccschem.021.202000768.
(5) Xu, F. F.; Li, Y. J.; Lv, Y.; Dong, H.; Lin, X.; Wang, K.; Yao, J.; Zhao, Y. S. Flat-Panel Laser Displays Based on Liquid Crystal Microlaser Arrays. *CCS Chemistry* **2020**, *2* (6), 369-375. DOI: 10.31635/ccschem.020.202000162.
(6) Periyanagounder, D.; Wei, T. C.; Li, T. Y.; Lin, C. H.; Goncalves, T. P.; Fu, H. C.; Tsai, D. S.; Ke, J. J.; Kuo, H. W.; Huang, K. W.; et al. Fast-Response, Highly Air-Stable, and Water-Resistant Organic Photodetectors Based on a Single-Crystal Pt Complex. *Adv Mater* **2020**, *32* (2), e1904634. DOI: 10.1002/adma.201904634 From NLM PubMed-not-MEDLINE.
(7) <sciadv.1700225.pdf>.
(8) An, M. H.; Ding, R.; Zhu, Q. C.; Ye, G. D.; Wang, H.; Du, M. X.; Chen, S. N.; Liu, Y.; Xu, M. L.; Xu, T.; et al. Well‐Balanced Ambipolar Organic Single Crystals toward Highly Efficient Light‐Emitting Devices. *Advanced Functional Materials* **2020**, *30* (49). DOI: 10.1002/adfm.202002422.
(9) Ding, R.; Feng, J.; Dong, F. X.; Zhou, W.; Liu, Y.; Zhang, X. L.; Wang, X. P.; Fang, H. H.; Xu, B.; Li, X. B.; et al. Highly Efficient Three Primary Color Organic Single‐Crystal Light‐Emitting Devices with Balanced Carrier Injection and Transport. *Advanced Functional Materials* **2017**, *27* (13). DOI: 10.1002/adfm.201604659.
(10) Ding, R.; Wang, X. P.; Feng, J.; Li, X. B.; Dong, F. X.; Tian, W. Q.; Du, J. R.; Fang, H. H.; Wang, H. Y.; Yamao, T.; et al. Clarification of the Molecular Doping Mechanism in Organic Single-Crystalline Semiconductors and their Application in Color-Tunable Light-Emitting Devices. *Adv Mater* **2018**, *30* (43), e1801078. DOI: 10.1002/adma.201801078 From NLM PubMed-not-MEDLINE.
(11) Chandrasekar, R. Mechanophotonics - a guide to integrating microcrystals toward monolithic and hybrid all-organic photonic circuits. *Chem Commun (Camb)* **2022**, *58* (21), 3415-3428. DOI: 10.1039/d2cc00044j From NLM PubMed-not-MEDLINE.
(12) Wang, C.-H.; Gao, X.; Zhong, Y.-N.; Liu, J.; Xu, J.-L.; Wang, S.-D. Controlled surface doping for operating stability enhancement in organic field-effect transistors. *Organic Electronics* **2017**, *42*, 367-371. DOI: 10.1016/j.orgel.2016.12.051.
(13) Sun, Z.; Liu, Z.; Li, J.; Tai, G. A.; Lau, S. P.; Yan, F. Infrared photodetectors based on CVD-grown graphene and PbS quantum dots with ultrahigh responsivity. *Adv Mater* **2012**, *24* (43), 5878-5883. DOI: 10.1002/adma.201202220 From NLM Medline.
(14) Su, B.; Liu, X.; Peng, X.; Xiao, T.; Su, Z. Preparation and characterization of the TiO2/polymer complex nanomaterial. *Materials Science and Engineering: A* **2003**, *349* (1-2), 59-62. DOI: 10.1016/s0921-5093(02)00544-0.
(15) Ramgir, N.; Bhusari, R.; Rawat, N. S.; Patil, S. J.; Debnath, A. K.; Gadkari, S. C.; Muthe, K. P. TiO2/ZnO heterostructure nanowire based NO2 sensor. *Materials Science in Semiconductor Processing* **2020**, *106*.

DOI: 10.1016/j.mssp.2019.104770.
(16) Xu, Y.; Li, G.; Li, R.; Jing, Y.; Zhang, H.; Wang, X.; Du, Z.; Wu, J.; Lan, Z. PbS/CdS heterojunction thin layer affords high-performance carbon-based all-inorganic solar cells. *Nano Energy* **2022**, *95*. DOI: 10.1016/j.nanoen.2022.106973.
(17) Pei, K.; Zhai, T. Emerging 2D Organic-Inorganic Heterojunctions. *Cell Reports Physical Science* **2020**, *1* (8). DOI: 10.1016/j.xcrp.2020.100166.
(18) Laquai, F.; Park, Y. S.; Kim, J. J.; Basche, T. Excitation energy transfer in organic materials: from fundamentals to optoelectronic devices. *Macromol Rapid Commun* **2009**, *30* (14), 1203-1231. DOI: 10.1002/marc.200900309 From NLM PubMed-not-MEDLINE.
(19) Ravi, J.; Kumar, A. V.; Karothu, D. P.; Annadhasan, M.; Naumov, P.; Chandrasekar, R. Geometrically Reconfigurable, 2D, All‐Organic Photonic Integrated Circuits Made from Two Mechanically and Optically Dissimilar Crystals. *Advanced Functional Materials* **2021**, *31* (43). DOI: 10.1002/adfm.202105415.
(20) Yu, J.; Mu, C.; Yan, B.; Qin, X.; Shen, C.; Xue, H.; Pang, H. Nanoparticle/MOF composites: preparations and applications. *Materials Horizons* **2017**, *4* (4), 557-569. DOI: 10.1039/c6mh00586a.
(21) Li, Z. Z.; Wu, J. J.; Wang, X. D.; Wang, K. L.; Zhang, S.; Xie, W. F.; Liao, L. S. Controllable Fabrication of In‐Series Organic Heterostructures for Optical Waveguide Application. *Advanced Optical Materials* **2019**, *7* (19). DOI: 10.1002/adom.201900373.
(22) Zhuo, M.-P.; He, G.-P.; Yuan, Y.; Tao, Y.-C.; Wei, G.-Q.; Wang, X.-D.; Lee, S.-T.; Liao, L.-S. Super-Stacking Self-Assembly of Organic Topological Heterostructures. *CCS Chemistry* **2021**, *3* (1), 413-424. DOI: 10.31635/ccschem.020.202000171.
(23) Annadhasan, M.; Karothu, D. P.; Chinnasamy, R.; Catalano, L.; Ahmed, E.; Ghosh, S.; Naumov, P.; Chandrasekar, R. Micromanipulation of Mechanically Compliant Organic Single-Crystal Optical Microwaveguides. *Angew Chem Int Ed Engl* **2020**, *59* (33), 13821-13830. DOI: 10.1002/anie.202002627 From NLM PubMed-not-MEDLINE.
(24) Chen, K.; Li, G.; Zhang, H.; Wu, H.; Li, Y.; Li, Y.; Wang, Z.; Tang, B. Z. Construction of sublimable pure organic ionic material with high solid luminescence efficiency based on anion-π+ interactions tuning strategy. *Chemical Engineering Journal* **2022**, *433*. DOI: 10.1016/j.cej.2021.133646.
(25) Kim, T.; Mun, J.; Park, H.; Joung, D.; Diware, M.; Won, C.; Park, J.; Jeong, S. H.; Kang, S. W. Wafer-scale production of highly uniform two-dimensional MoS(2) by metal-organic chemical vapor deposition. *Nanotechnology* **2017**, *28* (18), 18LT01. DOI: 10.1088/1361-6528/aa6958 From NLM PubMed-not-MEDLINE.
(26) Minari, T.; Lui, C.; Kano, M.; Tskukagoshi, K. Controlled self-assembly of organic semiconductors for solution-based fabrication of organic field-effect transistors. *Adv Mater* **2012**, *24* (2), 299-306. DOI: 10.1002/adma.201102554 From NLM Medline.
(27) Ravi, J.; Annadhasan, M.; Kumar, A. V.; Chandrasekar, R. Mechanically Reconfigurable Organic Photonic Integrated Circuits Made from Two Electronically Different Flexible Microcrystals. *Advanced Functional Materials* **2021**, *31* (25). DOI: 10.1002/adfm.202100642.
(28) Ravi, J.; Feiler, T.; Mondal, A.; Michalchuk, A. A. L.; Reddy, C. M.; Bhattacharya, B.; Emmerling, F.; Chandrasekar, R. Plastically Bendable Organic Crystals for Monolithic and Hybrid Micro‐Optical Circuits. *Advanced Optical Materials* **2022**, *11* (13). DOI: 10.1002/adom.202201518.
(29) <Wide-band_optical_communication_systems_Part_IIFrequency-division_multiplexing.pdf>.
(30) Zhang, C.; Zheng, J. Y.; Zhao, Y. S.; Yao, J. Organic core-shell nanostructures: microemulsion synthesis and upconverted emission. *Chem Commun (Camb)* **2010**, *46* (27), 4959-4961. DOI: 10.1039/c0cc00347f

From NLM PubMed-not-MEDLINE.
(31) Lei, Y.; Sun, Y.; Liao, L.; Lee, S. T.; Wong, W. Y. Facet-Selective Growth of Organic Heterostructured Architectures via Sequential Crystallization of Structurally Complementary pi-Conjugated Molecules. *Nano Lett* **2017**, *17* (2), 695-701. DOI: 10.1021/acs.nanolett.6b03778 From NLM PubMed-not-MEDLINE.
(32) Zhuo, M. P.; Wu, J. J.; Wang, X. D.; Tao, Y. C.; Yuan, Y.; Liao, L. S. Hierarchical self-assembly of organic heterostructure nanowires. *Nat Commun* **2019**, *10* (1), 3839. DOI: 10.1038/s41467-019-11731-7 From NLM PubMed-not-MEDLINE.
(33) Yao, W.; Han, G.; Huang, F.; Chu, M.; Peng, Q.; Hu, F.; Yi, Y.; Jiang, H.; Yao, J.; Zhao, Y. S. "H"-like Organic Nanowire Heterojunctions Constructed from Cooperative Molecular Assembly for Photonic Applications. *Adv Sci (Weinh)* **2015**, *2* (11), 1500130. DOI: 10.1002/advs.201500130 From NLM PubMed-not-MEDLINE.
(34) Pan, M.-L.; Wang, C.; Zhuo, M.-P.; Li, Z.-Z.; Yuan, Y.; Tao, Y.-C.; Wang, X.-D. Sequential Self-Assembly of Organic Heterostructured Architectures Composed of Low-Dimensional Microcrystals. *ACS Materials Letters* **2020**, *2* (6), 658-664. DOI: 10.1021/acsmaterialslett.0c00125.
(35) Yang, C.; Gu, L.; Ma, C.; Gu, M.; Xie, X.; Shi, H.; Ma, H.; Yao, W.; An, Z.; Huang, W. Controllable co-assembly of organic micro/nano heterostructures from fluorescent and phosphorescent molecules for dual anti-counterfeiting. *Materials Horizons* **2019**, *6* (5), 984-989. DOI: 10.1039/c8mh01582a.
(36) Tao, Y. C.; Wang, X. D.; Li, Z. Z.; Zhuo, M. P.; Yu, Y.; Yan, C. C.; Xie, W. F.; Liao, L. S. Fine Synthesis of Longitudinal/Horizontal‐Growth Organic Heterostructures for the Optical Logic Gates. *Advanced Electronic Materials* **2020**, *6* (4). DOI: 10.1002/aelm.201901268.
(37) Li, Z.-Z.; Tao, Y.-C.; Wang, X.-D.; Liao, L.-S. Organic Nanophotonics: Self-Assembled Single-Crystalline Homo-/Heterostructures for Optical Waveguides. *ACS Photonics* **2018**, *5* (9), 3763-3771. DOI: 10.1021/acsphotonics.8b00815.
(38) Pang, Y.; Liu, Y.; Gao, M.; Ouyang, L.; Liu, J.; Wang, H.; Zhu, M.; Pan, H. A mechanical-force-driven physical vapour deposition approach to fabricating complex hydride nanostructures. *Nat Commun* **2014**, *5*, 3519. DOI: 10.1038/ncomms4519 From NLM PubMed-not-MEDLINE.
(39) Pedersen, H.; Elliott, S. D. Studying chemical vapor deposition processes with theoretical chemistry. *Theoretical Chemistry Accounts* **2014**, *133* (5). DOI: 10.1007/s00214-014-1476-7.
(40) Ye, X.; Liu, Y.; Han, Q.; Ge, C.; Cui, S.; Zhang, L.; Zheng, X.; Liu, G.; Liu, J.; Liu, D.; et al. Microspacing In-Air Sublimation Growth of Organic Crystals. *Chemistry of Materials* **2018**, *30* (2), 412-420. DOI: 10.1021/acs.chemmater.7b04170.
(41) Xu, S.; Zhang, S.; Gao, H.; Kirch, J.; Botez, D.; Mawst, L. Strain-balanced InGaAs/AlInAs/InP quantum cascade laser grown on GaAs by MOVPE. *Journal of Crystal Growth* **2023**, *619*. DOI: 10.1016/j.jcrysgro.2023.127310.
(42) Pradeep, V. V.; Annadhasan, M.; Chandrasekar, R. Vapour-Phase Epitaxial Growth of Dual-Colour-Emitting DCM-Perylene Micro-Heterostructure Optical Waveguides. *Chem Asian J* **2019**, *14* (24), 4577-4581. DOI: 10.1002/asia.201901221 From NLM PubMed-not-MEDLINE.
(43) Hai, T.; Feng, Z.; Sun, Y.; Wong, W. Y.; Liang, Y.; Zhang, Q.; Lei, Y. Vapor-Phase Living Assembly of pi-Conjugated Organic Semiconductors. *ACS Nano* **2022**, *16* (2), 3290-3299. DOI: 10.1021/acsnano.1c11295 From NLM PubMed-not-MEDLINE.
(44) Lin, H. C.; Jin, B. Y. Charge-Transfer Interactions in Organic Functional Materials. *Materials (Basel)* **2010**, *3* (8), 4214-4251. DOI: 10.3390/ma3084214 From NLM PubMed-not-MEDLINE.
(45) Zheng, J. Y.; Yan, Y.; Wang, X.; Zhao, Y. S.; Huang, J.; Yao, J. Wire-on-wire growth of fluorescent organic heterojunctions. *J Am Chem Soc* **2012**, *134* (6), 2880-2883. DOI: 10.1021/ja209815f From NLM

PubMed-not-MEDLINE.
(46) Wang, B.; Fu, X.; Song, S.; Chu, H. O.; Gibson, D.; Li, C.; Shi, Y.; Wu, Z. Simulation and Optimization of Film Thickness Uniformity in Physical Vapor Deposition. *Coatings* **2018**, *8* (9). DOI: 10.3390/coatings8090325.
(47) <便宜.pdf>.
(48) <轻.pdf>.
(49) Ariga, K.; Hill, J. P.; Lee, M. V.; Vinu, A.; Charvet, R.; Acharya, S. Challenges and breakthroughs in recent research on self-assembly. *Sci Technol Adv Mater* **2008**, *9* (1), 014109. DOI: 10.1088/1468-6996/9/1/014109 From NLM PubMed-not-MEDLINE.
(50) Liu, X. T.; Wang, K.; Chang, Z.; Zhang, Y. H.; Xu, J.; Zhao, Y. S.; Bu, X. H. Engineering Donor-Acceptor Heterostructure Metal-Organic Framework Crystals for Photonic Logic Computation. *Angew Chem Int Ed Engl* **2019**, *58* (39), 13890-13896. DOI: 10.1002/anie.201906278 From NLM PubMed-not-MEDLINE.
(51) Hou, Y.; Gao, Z.; Zhao, Y. S.; Yan, Y. Organic micro/nanoscale materials for photonic barcodes. *Organic Chemistry Frontiers* **2020**, *7* (18), 2776-2788. DOI: 10.1039/d0qo00613k.
(52) Xu, C.-F.; Yang, W.-Y.; Lv, Q.; Wang, X.-D.; Liao, L.-S. Directed self-assembly of organic crystals into chip-like heterostructures for signal processing. *Science China Materials* **2022**, *66* (2), 733-739. DOI: 10.1007/s40843-022-2210-9.
(53) Kong, Q.; Liao, Q.; Xu, Z.; Wang, X.; Yao, J.; Fu, H. Epitaxial self-assembly of binary molecular components into branched nanowire heterostructures for photonic applications. *J Am Chem Soc* **2014**, *136* (6), 2382-2388. DOI: 10.1021/ja410069k From NLM PubMed-not-MEDLINE.
(54) Gao, Z.; Xu, B.; Zhang, T.; Liu, Z.; Zhang, W.; Sun, X.; Liu, Y.; Wang, X.; Wang, Z.; Yan, Y.; et al. Spatially Responsive Multicolor Lanthanide-MOF Heterostructures for Covert Photonic Barcodes. *Angew Chem Int Ed Engl* **2020**, *59* (43), 19060-19064. DOI: 10.1002/anie.202009295 From NLM PubMed-not-MEDLINE.
(55) Sun, M. J.; Liu, Y.; Yan, Y.; Li, R.; Shi, Q.; Zhao, Y. S.; Zhong, Y. W.; Yao, J. In Situ Visualization of Assembly and Photonic Signal Processing in a Triplet Light-Harvesting Nanosystem. *J Am Chem Soc* **2018**, *140* (12), 4269-4278. DOI: 10.1021/jacs.7b12519 From NLM PubMed-not-MEDLINE.
(56) Zheng, J. Y.; Xu, H.; Wang, J. J.; Winters, S.; Motta, C.; Karademir, E.; Zhu, W.; Varrla, E.; Duesberg, G. S.; Sanvito, S.; et al. Vertical Single-Crystalline Organic Nanowires on Graphene: Solution-Phase Epitaxy and Optical Microcavities. *Nano Lett* **2016**, *16* (8), 4754-4762. DOI: 10.1021/acs.nanolett.6b00526 From NLM PubMed-not-MEDLINE.
(57) Fang, X.; Yang, X.; Yan, D. Vapor-phase π–π molecular recognition: a fast and solvent-free strategy towards the formation of co-crystalline hollow microtube with 1D optical waveguide and up-conversion emission. *Journal of Materials Chemistry C* **2017**, *5* (7), 1632-1637. DOI: 10.1039/c6tc05048d.
(58) Ding, L.; Wang, Z. Y.; Wang, J. Y.; Pei, J. Organic Semiconducting Materials Based on BDOPV: Structures, Properties, and Applications. *Chinese Journal of Chemistry* **2019**, *38* (1), 13-24. DOI: 10.1002/cjoc.201900347.
(59) Huang, Y.; Wang, Z.; Chen, Z.; Zhang, Q. Organic Cocrystals: Beyond Electrical Conductivities and Field-Effect Transistors (FETs). *Angew Chem Int Ed Engl* **2019**, *58* (29), 9696-9711. DOI: 10.1002/anie.201900501 From NLM PubMed-not-MEDLINE.
(60) <ajayaghosh-praveen-2007-π-organogels-of-self-assembled-p-phenylenevinylenes-soft-materials-with-distinct-size-shape-and.pdf>.
(61) <etter-2002-hydrogen-bonds-as-design-elements-in-organic-chemistry.pdf>. DOI: 10.1021/j100165a007,.

(62) <离子注入介绍.pdf>.
(63) Bolla, G.; Liao, Q.; Amirjalayer, S.; Tu, Z.; Lv, S.; Liu, J.; Zhang, S.; Zhen, Y.; Yi, Y.; Liu, X.; et al. Cocrystallization Tailoring Multiple Radiative Decay Pathways for Amplified Spontaneous Emission. *Angew Chem Int Ed Engl* **2021**, *60* (1), 281-289. DOI: 10.1002/anie.202007655 From NLM PubMed-not-MEDLINE.
(64) <lucassen-et-al-2007-co-crystallization-of-sym-triiodo-trifluorobenzene-with-bipyridyl-donors-consistent-formation-of.pdf>.
(65) Dai, W.; Niu, X.; Wu, X.; Ren, Y.; Zhang, Y.; Li, G.; Su, H.; Lei, Y.; Xiao, J.; Shi, J.; et al. Halogen Bonding: A New Platform for Achieving Multi-Stimuli-Responsive Persistent Phosphorescence. *Angew Chem Int Ed Engl* **2022**, *61* (13), e202200236. DOI: 10.1002/anie.202200236 From NLM PubMed-not-MEDLINE.
(66) d'Agostino, S.; Grepioni, F.; Braga, D.; Ventura, B. Tipping the Balance with the Aid of Stoichiometry: Room Temperature Phosphorescence versus Fluorescence in Organic Cocrystals. *Crystal Growth & Design* **2015**, *15* (4), 2039-2045. DOI: 10.1021/acs.cgd.5b00226.
(67) Liu, H.; Lu, Z.; Zhang, Z.; Wang, Y.; Zhang, H. Highly Elastic Organic Crystals for Flexible Optical Waveguides. *Angew Chem Int Ed Engl* **2018**, *57* (28), 8448-8452. DOI: 10.1002/anie.201802020 From NLM PubMed-not-MEDLINE.
(68) Halabi, J. M.; Ahmed, E.; Catalano, L.; Karothu, D. P.; Rezgui, R.; Naumov, P. Spatial Photocontrol of the Optical Output from an Organic Crystal Waveguide. *J Am Chem Soc* **2019**, *141* (38), 14966-14970. DOI: 10.1021/jacs.9b07645 From NLM PubMed-not-MEDLINE.
(69) Liu, B.; Di, Q.; Liu, W.; Wang, C.; Wang, Y.; Zhang, H. Red-Emissive Organic Crystals of a Single-Benzene Molecule: Elastically Bendable and Flexible Optical Waveguide. *J Phys Chem Lett* **2019**, *10* (7), 1437-1442. DOI: 10.1021/acs.jpclett.9b00196 From NLM PubMed-not-MEDLINE.
(70) Huang, R.; Tang, B.; Ye, K.; Wang, C.; Zhang, H. Flexible Luminescent Organic Bulk Crystal: 2D Elasticity toward 3D Optical Waveguide. *Advanced Optical Materials* **2019**, *7* (22). DOI: 10.1002/adom.201900927.
(71) Lu, Z.; Zhang, Y.; Liu, H.; Ye, K.; Liu, W.; Zhang, H. Optical Waveguiding Organic Single Crystals Exhibiting Physical and Chemical Bending Features. *Angew Chem Int Ed Engl* **2020**, *59* (11), 4299-4303. DOI: 10.1002/anie.201914026 From NLM PubMed-not-MEDLINE.
(72) Annadhasan, M.; Agrawal, A. R.; Bhunia, S.; Pradeep, V. V.; Zade, S. S.; Reddy, C. M.; Chandrasekar, R. Mechanophotonics: Flexible Single-Crystal Organic Waveguides and Circuits. *Angew Chem Int Ed Engl* **2020**, *59* (33), 13852-13858. DOI: 10.1002/anie.202003820 From NLM PubMed-not-MEDLINE.